ISBN: 978-3-95450-241-7 ISSN: 2673-5350 doi:10.18429/JACoW-IBIC2022-WEP20

# EMITTANCE DIAGNOSTICS AT PETRA IV

M. Marongiu*, G. Kube, M. Lantschner, A. Novokshonov, K. Wittenburg
Deutsches Elektronen-Synchrotron DESY, Germany

*Abstract*

The PETRA IV project will be a Diffraction Limited Light Source designed to be the successor of PETRA III, the 6 GeV 3rd generation hard X-Ray synchrotron light source at DESY in Hamburg. It will operate at a beam energy of 6 GeV with a design emittance of 20/4 pm rad. For a precise emittance online control, two dedicated diagnostics beamlines will be built up to image the beam profile with synchrotron radiation in the X-Ray region. With two beamlines, it will be possible to extract both the transverse beam emittances and the beam energy spread. Both beamlines will be equipped with two interchangeable X-Ray optical systems: a pinhole camera system to achieve high dynamic range and a Fresnel Diffractometry system for high resolution measurements in the range 1-18 µm. This paper describes the planned setup and deals with the possible limitations.

## INTRODUCTION

The PETRA IV project [1] will be a Diffraction Limited Light Source designed to be the successor of PETRA III, the 6 GeV 3rd generation hard X-Ray synchrotron light source at DESY in Hamburg. It will operate at a beam energy of 6 GeV with a design emittance of 20/4 pm rad instead of the 1300/10 pm rad currently obtained in PETRA III. The machine will be installed in the same tunnel of the current operating one. Table 1 summarizes the main parameters of PETRA IV and PETRA III.

Table 1: Main Parameters of PETRA IV Compared with the Values Currently in Use at PETRA III

| Parameters | PETRA IV | Petra III |
|---|---|---|
| Energy (GeV) | 6 | 6 |
| Circumference (m) | 2304 | 2304 |
| Current (mA) | 80/200 | 100/120 |
| Number bunches | 80/1600 | 40/480 |
| Emittance (pm rad) | | |
| Horizontal | <20 | 1300 |
| Vertical | <4 | 10 |
| # Undulator beamlines | 30 | 21 (26) |

For a precise emittance online control, two dedicated diagnostics beamlines will be built up to image the beam profile with synchrotron radiation in the X-Ray region. With two beamlines in locations with different dispersion, it will be possible to extract both the transverse beam emittances and the beam energy spread. The emittance sensitivity required is 0.5 pm rad which translates in a beam size sensitivity requirement of 100 nm.

* marco.marongiu@desy.de

It will be also required to have a high dynamic range measurement; therefore, each beamline will be equipped also with an X-Ray pinhole camera system (XPC) to measure beam size above 15 µm. Figure 1 shows a sketch of the designed beamline. The overall beamline length of about 50 m derives from the requirement to place the detector part outside the accelerator tunnel.


Figure 1: Beamline sketch of the emittance measurement.

Different locations for the beamlines have been considered and, due to geometric constraints, it has been chosen a canted section using as a radiation source a 3 Pole Wiggler (3PW) with a peak magnetic field of around 0.8 T. Table 2 shows the main beam parameters at the beamline locations.

Table 2: Main beam parameters at the possible beamlines locations. The last column represents the relative dispersion contribution to the emittance. The 3 pole wiggler (3PW) considered has a peak magnetic field of around 0.8 T.

| Rad. Source | $\beta_x$ m | $\beta_y$ m | $\sigma_x$ µm | $\sigma_y$ µm | D. % |
|---|---|---|---|---|---|
| 3PW | 4.6 | 4.6 | 9.6 | 4.3 | 0.04 |
| 3PW | 2.6 | 2.6 | 8.1 | 3.3 | 10.3 |

## X-RAY FRESNEL DIFFRACTOMETRY

In order to achieve a high resolution measurement, the X-Ray Fresnel diffractometry technique [2] (XFD) has been considered. Optimizing opportunely a single slit width ($A$), a double-lobed pattern emerges and the depth of its median dip is correlated to the source size (i.e. the dip becomes shallow with the increase of the source size). Figure 2 shows a sketch of the technique: the choices of the distance of the slit to the source point ($L$), the distance from the slit to the observation point ($R$) and the observing wavelength ($\lambda$) determine the slit width. The only requirement for the light

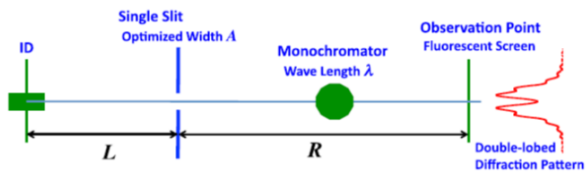


Figure 2: Sketch of the XFD measurement [2].

ISBN: 978-3-95450-241-7 ISSN: 2673-5350 doi:10.18429/JACoW-IBIC2022-WEP20

source is that the radiation should be a spherical wave with a flux distribution wider than the slit width.

Under these assumptions, the Point Spread Function (PSF) at the observation point can be expressed by Eq. (1).

$$I(y, y_e) \propto \left| \int_{-A/2}^{A/2} \sqrt{I_s(y_s - y_e)} \exp\left[ j \frac{\pi}{\lambda} \frac{R+L}{RL} \left[ (y_s - y_e) - \frac{L(y - y_e)}{L+R} \right]^2 \right] dy_s \right|^2, \quad (1)$$

where $I_s(y_s - y_e)$ is the flux intensity distribution of radiation at the slit, $y_e$ is the electron position at the source point, $y_s$ and $y$ are the coordinates on the slit and the observation point, respectively.

Assuming an electron position at the source $y_e = 0$ and a constant flux distribution, Eq. (1) can be written as in Eq. (2).

$$\begin{aligned} N1 &= (R+L)A/2, \\ D &= \frac{\sqrt{RL\lambda(R+L)}}{(-1)^{1/4}\sqrt{\pi}}, \\ I(y) &\approx \left| \frac{(-1)^{3/4}\sqrt{\lambda RL}}{2\sqrt{R+L}} \left[ Erfi\left( \frac{(-N1 - Ly)}{D} \right) \right. \right. \\ &\quad \left. \left. - Erfi\left( \frac{(N1 - Ly)}{D} \right) \right] \right|^2. \end{aligned} \quad (2)$$

The optimised aperture is obtained applying the condition of destructive interference of the light contributing to the center of the PSF ($y = 0$) and can be expressed as in Eq. (3).

$$A = \sqrt{7\lambda \frac{LR}{L+R}}. \quad (3)$$

The XFD scheme requires a monochromatic X-Ray: therefore, a Silicon (111) is considered to be used as a monochromator crystal since it generates a photon bandwidth narrow enough ($\approx 10^{-4}$).

The peak-to-valley intensity ratio is correlated to the beam source size: this correlation is particularly strong in a small interval of less than 20 µm (i.e. from 1 µm to 20 µm) where the sensibility to beam size variations reaches the sub-micron order. The precise values of sensitivities and dynamic range are related to the choice of the beamline parameters ($\lambda$, $L$, $R$).

For instance, Fig. 3 shows the sensitivity curves for different photon energies: it can be seen that lower energies correspond to higher dynamic range but also to lower sensitivity to small beam size changes. Indeed, the slope of the curves increases with the energy. Similar studies can be done varying the other beamline parameters: for instance, an increase of $L$ or of $R$ causes an increase of the dynamic range at the expense of the sensitivity.

For a quantitative estimation, one can evaluate the derivative of the sensitivity curves of Fig. 3 and observe in which

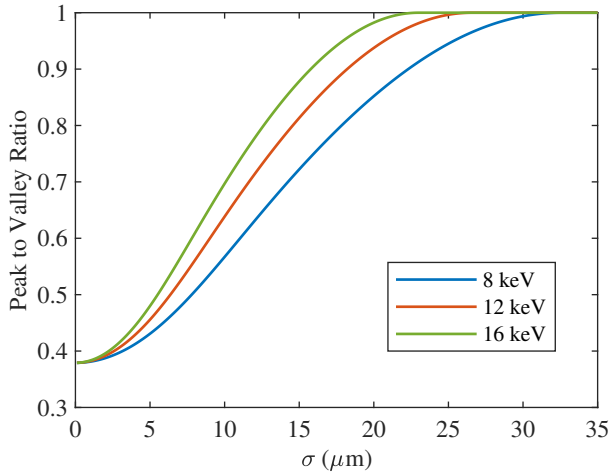


Figure 3: Sensitivity curves for three different observing photon energies. The curves are calculated considering $L = R = 20$ m and optimizing $A$ for each energy according to Eq. (3).

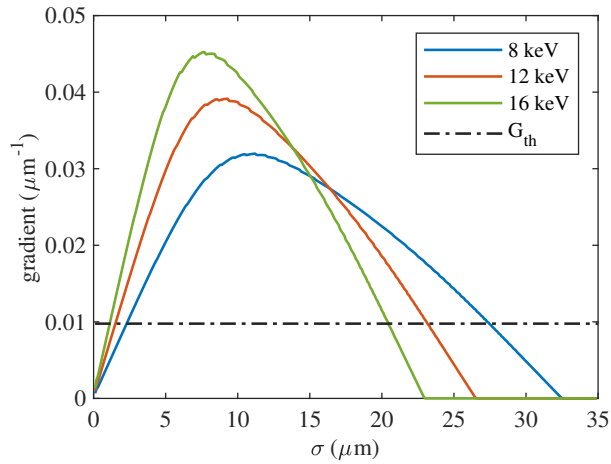


Figure 4: Derivatives of the sensitivity curves for three different observing photon energies. The sensitivity curves are calculated considering $L = R = 20$ m and optimizing $A$ for each energy according to Eq. (3). The dash-dotted line represents the threshold value calculated for a sensitivity requirement of 100 nm and a camera sensor of 10 effective bits.

beam size range the derivatives are above a certain threshold. This threshold will be inversely proportional to the maximum sensitivity required and to the number of bits the camera sensor uses to digitize the intensity, as seen in Fig. 4. Hence, an increase of the number of bits of the sensor, or a more relaxed sensitivity requirement, allows a higher dynamic range.

Given the PETRA IV requirements, a possible solution is to place a slit at 30 m from the radiation source and the detector at 20 m from the slit selecting with a monochromator a photon energy of 16 keV; the optimized aperture value is 81 µm. This system is able to detect 100 nm beam size variation in a range between 1 µm and 18.9 µm assuming a camera sensor with 10 effective bits.

ISBN: 978-3-95450-241-7 ISSN: 2673-5350 doi:10.18429/JACoW-IBIC2022-WEP20



## X-RAY PINHOLE CAMERA

In order to be able to measure with a higher dynamic range, also an X-Ray pinhole camera (XPC) will be implemented. The PSF is calculated in the image plane based on numerical near field calculations with the code SRW [3]. As a possible solution it is planned to place the pinhole at 10 m from the radiation source and, hence, at 40 m from the observation point; the pinhole aperture, optimized for a photon energy of 16 keV, is equal to 24 µm and the PSF rms size is 11 µm. Figure 5 shows the vertical profile of the PSF.

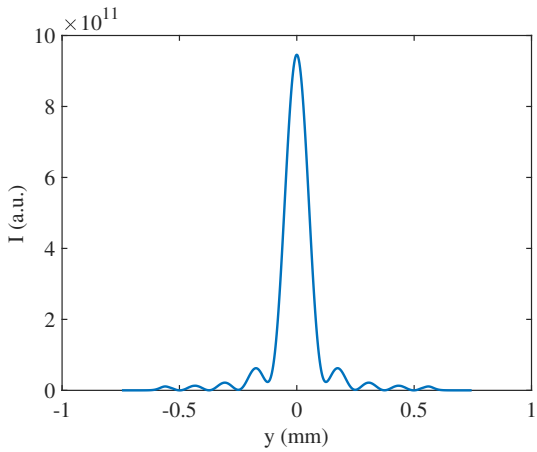


Figure 5: Vertical profile of the XPC PSF. The curve is calculated considering $L = 10$ m, $R = 40$ m, $E = 16$ keV and $A = 24$ µm.

One of the main issues regarding the XPC technique is the proper manufacturing of the pinhole target: indeed, in order to avoid the use of background subtraction techniques, the target must be thick enough (i.e. typically above 1 mm for radiation up to 60 keV) as shown in Fig. 6. Three materials have been considered: gold which was already tested at DIAMOND [4], the commonly used tungsten and tungsten carbide [5]. The transmission coefficient data, obtained with the simulation code SPECTRA [6], show that a 1 mm thickness could be sufficient in the case of gold and tungsten and a photon energy range below 60 keV; tungsten carbide requires instead a larger thickness (1.3 mm). The manufacture of a small aperture (about 25 µm) in a thick material (1 mm or more) is challenging: hence, different manufacturing techniques have been considered. At DIAMOND [4], a LIGA technique has been tested, however it is limited to about 250 µm thickness. Laser drilling results in a more suitable solution for thick material: a 20 µm hole in 1 mm gold target has been already produced successfully and will be tested in the near future. Studies for 2 mm thick material are ongoing.

Finally, it is fundamental to properly estimate the different contributions to the beam size measurement: indeed, the PSF of the pinhole, the PSF of the optical system and eventual misalignment contribute to the beam size measurement by adding in quadrature to the real rms beam size. A method to estimate all this contribution takes advantage of

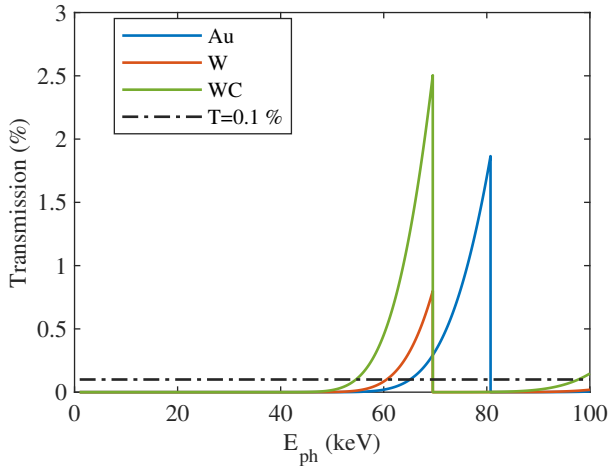


Figure 6: Transmission coefficient as a function of the photon energy for three different materials each one 1 mm thick. The blue curve represents gold, the red curve represents tungsten and the green one tungsten carbide. The dash-dotted curve represent the 0.1% threshold above which a background subtraction technique is required. Data calculated with the simulation code SPECTRA [6].

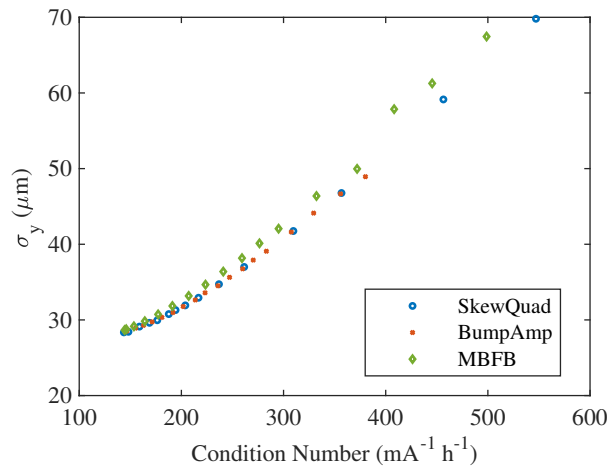


Figure 7: Measured rms vertical beam size as a function of the condition number. The blue circles represent the skew quadrupole case; the red dots represent the bump amplitude case and the green diamond the noise in the MBFB case.

the linear proportionality of the vertical beam size with the beam lifetime in Touschek dominated machine [4]. Three different sets of data have been taken at PETRA III to perform this evaluation: in the first one, the beam lifetime has been changed acting on the skew quadrupoles. In the second case, a localized symmetric dispersion bump in a damping wiggler has been used and in the last case, a white noise generator in the Multi Bunch Feedback (MBFB) has been used instead. Figure 7 shows a perfect overlapping of the first two data sets, while the third one shows a slightly different behaviour. However, the analysis of the full data is still ongoing.

ISBN: 978-3-95450-241-7 ISSN: 2673-5350 doi:10.18429/JACoW-IBIC2022-WEP20

## CONCLUSION

The article summarizes the emittance diagnostic beamline setups that are currently planned for the PETRA IV machine. The possibility to observe beam size variation as small as 100 nm in a range between 1 µm and 18.9 µm is shown. To achieve a high dynamic range, a pinhole camera will be also installed. The article also deals with some possible limitations like the maximum aspect ratio achievable for the pinhole target with the currently available manufacturing techniques. Some prototypes are ready to be installed and tested in the PETRA III machine.

## ACKNOWLEDGEMENT

The PETRA IV project team acknowledges funding of the technical design phase granted by the Behörde für Wissenschaft, Forschung, Gleichstellung und Bezirke (BWFGB) of the Freie und Hansestadt Hamburg, as well as by the Bundesministerium für Bildung und Forschung (BMBF) under the contract DES21TDR.

## REFERENCES

[1] C. G. Schroer *et al.*, "PETRA IV: The ultralow-emittance source project at DESY," *J. Synchrotron Radiat.*, vol. 25, no. 5, pp. 1277–1290, 2018. doi:10.1107/S1600577518008858

[2] M. Masaki, S. Takano, M. Takao, and Y. Shimosaki, "X-Ray Fresnel diffractometry for ultralow emittance diagnostics of next generation synchrotron light sources," *Phys. Rev. Spec. Top. Accel Beams*, vol. 18, no. 4, p. 042 802, 2015. doi:10.1103/PhysRevSTAB.18.042802

[3] O. Chubar and P. Elleaume, "Accurate and Efficient Computation of Synchrotron Radiation in the Near Field Region," in *Proc. EPAC'98*, Stockholm, Sweden, Jun. 1998. https://jacow.org/e98/papers/THP01G.pdf

[4] L. M. Bobb and G. Rehm, "Beam Size Measurement Using High Aspect Ratio LIGA Apertures in an X-Ray Pinhole Camera," in *Proc. IPAC'17*, Copenhagen, Denmark, May 2017, pp. 445–447. doi:10.18429/JACoW-IPAC2017-MOPAB132

[5] F. Ewald, "Emittance measurement at ESRF-EBS with the X-Ray pinhole," presented at the Elettra 2.0 Workshop on Optical Diagnostics for Low-Emittance Storage Rings, 2022.

[6] T. Tanaka, "Major upgrade of the synchrotron radiation calculation code SPECTRA," *J. Synchrotron Radiat.*, vol. 28, no. 4, pp. 1267–1272, 2021. doi:10.1107/S1600577521004100